PAGEOPH, manuscript No.
(will be inserted by the editor)

Effect of clay and mineralogy on permeability

José M. Carcione[1,2] · Davide Gei[1] · Ting Yu[2] · Jing Ba[2]

the date of receipt and acceptance should be inserted later

Abstract Absolute rock permeability depends on several factors, mainly porosity, ϕ, the geometry of the pore network (tortuosity), and the grain geometry, dimension and composition. The mineralogy composition plays an important role, mostly clay, which involves several components such as illite, smectite, kaolinite and chlorite. The presence of quartz and feldspar increases permeability, while clay minerals and calcite tend in the opposite direction. Basically, permeability decreases with a smaller grain radius, increasing tortuosity of the pore space and decreasing porosity. As the specific surface area of the pores increases, permeability decreases. Here, we compare four expressions for permeability based on clay content, grain dimension, tortuosity and mineral composition. All the expressions contain somehow the Kozeny-Carman (KC) factor $\phi^3/(1-\phi)^2$, which is obtained on physical grounds, and rely on fitting parameters related to the geometrical characteristics of the rock and its composition. Herron model is based on geochemical mineralogy composition. Despite the highly idealizations on which these models are based, the results indicate the prediction power of the Kozeny-Carman equation, provided that proper calibration is performed.

Keywords Permeability · Kozeny-Carman factor · Clay content · Grain size · Tortuosity · Mineralogy

1 Introduction

Permeability is important in groundwater flow (Neuzil, 1994), hydrocarbon production and CO_2 storage activities. During the last 30 years, the success of CO_2 storage rely on

[1]Istituto Nazionale di Oceanografia e di Geofisica Sperimentale (OGS), Borgo Grotta Gigante 42c, 34010 Sgonico, Trieste, Italy. E-mail: jcarcione@inogs.it
[2] School of Earth Sciences and Engineering, Hohai University, Nanjing, 211100, China.

a good estimation of permeability in the reservoir and mainly on the seal caprock and overburden to avoid possible leakages (Savioli et al., 2016). Low permeability is required in this case and this strongly depends on clay content and mineralogy. Permeability is also key factor in levee breach flood disasters, since levees in a river may collapse due to the condition of the soils (high permeability zones) that form the embankments (Sinha et al., 2017).

Fine-grain sediments, mud and its lithified versions (mudstone and shale), form approximately 70 % of the sedimentary basins. The permeability of shales is several orders of magnitude lower than that of coarser grain rocks, such as sandstone. Therefore, shales and even sandstones with a moderate amount of clay content (shaley sandstones) control the flow at which fluids move in the underground. Clay can reduce the porosity, increase the tortuosity and block the pore throats.

Knowing clay content, defined here as the volume fraction of particles less than 4 μm in diameter, is required to obtain reliable values of permeability, since this is strongly correlated with the grain and pore size distributions. To describe permeability, we use Kozeny-Carman type equations (Kozeny, 1927; Carman, 1961; Tiab and Donaldson, 2012) based on grain size, tortuosity and clay content, which implicitly involves several minerals, such as kaolinite, illite and smectite. Herron (1987) used explicit mineralogical information available from geochemistry to obtain estimates of both porosity and permeability. He quantified the effects of the minerals composing the rock by defining specific weights. These are positive for quartz and feldspar, negative for cements such as calcite or other carbonates, and negative for the clay minerals. The derived permeability logs obtained by Herron show good agreement with air permeabilities measured on core samples. Recently, Ma (2015) reviews permeability models, other than the Kozeny-Carman equations, based on power-law, exponential and polynomial dependences of porosity. Al Ismail and Zoback (2016) investigated the effect of mineralogy in experiments on organic shale samples, where they mainly considered clay and calcite (illite was the predominant clay mineral). They found that shale mineralogy did not show a clear effect on the magnitude of permeability. However, caution is required when interpreting permeability based on the Kozeny-Carman equation, since there is no one-to-one relation between porosity and permeability, because porosity is invariant under a homothetic transformation of the pore space (e.g., uniform, isotropic stretching), whereas permeability is not (Bernabé et al., 2003).

One important effect to consider when using permeability models is that permeability obtained with gas may yield higher values than that based on liquids. The difference between gas and fluid permeabilities is due to the Klinkenberg effect (e.g., Tanikawa and Shimamoto, 2006). This effect is important at low pressures and is due to the slip

flow of gas at pore walls, which enhances the gas flow, mainly when the pore sizes are very small, so it can be important in shales. In this case, the physical laws leading to the Kozeny-Carman (KC) equation do not hold and a correction has to be applied.
Here, we consider four models of permeability, which are generalizations of the Kozeny-Carman equation that incorporate clay content. The grain radii and tortuosity, besides the KC porosity factor, are the parameters of three of these models, whereas the fourth equation is based on mineralogy (Herron, 1987). Comparisons among these models and with experimental datasets are carried out in order to analyze the performance of the permeability expressions.

2 Permeability based on grain radii and tortuosity

Permeability can be described by the Kozeny-Carman equation (see Appendix A, where a demonstration is given). In this section, we present three different models, based on grain radii, tortuosity and specific surface area. We assume that the radius of the sand particles is much greater than the radius of the clay particles, at least a factor five.

2.1 Model 1

A simple model introduced by Carcione et al. (2000) assumes that a medium composed of clay and sand grains of single porosity ϕ and clay content C has the partial permeabilities given in equation (B.6) (Appendix B). There is permeability anisotropy, with the vertical component dominating the flow. The permeability components are determined by an analogy with a parallel and series connections of electrical resistances (horizontal and vertical component, respectively), as shown in Figures 1a and 1b, respectively, assuming that permeability is analogous to the inverse of the electrical resistance. Similarly, this distinction between horizontal and vertical permeability can be obtained from an analogy with the Backus average of the shear moduli parallel and perpendicular to layering (Backus, 1962; Carcione, 2014).
Strictly, the horizontal component is given by $\kappa_h = (1 - C)\kappa_s + C\kappa_c$, which from equations (B.3) and (B.6) does not depend on the clay content and is equal to the $C = 0$ curve (no matter the amount of clay, the fluid will flow through the less resistant element of the parallel connection, i.e., mainly through the sand component). This assumption is too strong and can give unrealistic values of the permeability anisotropy for $r_s \gg r_c$, where r_s and r_c are the radii of the sand and clay particles, respectively. A suitable model is to assume that the sandy part is affected by a given fraction of clay, say α. Then, according to the electric circuit shown in Figure 1a, the horizontal

component is given by

$$\kappa_h = (1 - C)\left(\frac{1 - \alpha C}{\kappa_s} + \frac{\alpha C}{\kappa_c}\right)^{-1} + C\kappa_c. \qquad (1)$$

A value of $\alpha = 0.2$ yields anisotropy levels in agreement with experimental data if $r_s = 50$ μm and $r_c = 1$ μm (Clennell et al., 1999; Adams et al., 2016).
On the other hand, the average (inverse) vertical permeability of the composite medium satisfies

$$\frac{1}{\kappa_v} = \frac{1 - C}{\kappa_s} + \frac{C}{\kappa_c} = \frac{(1-\phi)^2}{a\phi^3}\left[(1 - C)^2 + C^2 b^2\right], \qquad (2)$$

where $a = r_s^2/45$ and $b = r_s/r_c$, but in practice they are used as free parameters obtained from calibration of available data. These parameters contain information about the geometrical characteristics of the rock frame, such as the mean radius of the grains and the effective tortuosity $\mathcal{T}$ of the sand/clay frame network. Actually the factor 45 has been obtained in Appendix B as 18 $\mathcal{T}$, with $\mathcal{T} = 2.5$, which is an idealization for spherical grains, but one cannot expect to fit real data by considering a and b a result of such an ideal assumption.

2.2 Model 2

The more used model of permeability is usually given in terms of tortuosity,

$$\kappa = \frac{r_g^2\phi^3}{18\mathcal{T}(1-\phi)^2} \qquad (3)$$

(see demonstration in Appendix A), where

$$r_g^{-1} = C r_c^{-1} + (1 - C) r_s^{-1} \qquad (4)$$

is the average grain radius (Dullien, 1991) and $\mathcal{T}$ is the tortuosity defined in equation (A.10) and given by equations (A.16) and (A.19) for specific topologies of the pore space, namely, 3D interpenetrating tubes and solid particles flowing in a fluid, respectively. Equation (4) assumes that the densities of the sand and clay particles are the same.

2.3 Model 3

A well known model to obtain the permeability of sand/clay mixtures is that of Marion (1990), which considers that the two rock components have their own porosities, ϕ_s and ϕ_c, specific surface areas, s_s and s_c, and tortuosities, $\mathcal{T}_s$ and $\mathcal{T}_c$, respectively, for sand and clay. In sandstone and shaley sandstone, the clay minerals are located within the sand pore space, while for shale and sandy shale, clay is the frame and the sand grains are dispersed.

The expressions for permeability are based on equations (A.13), (A.14) and (A.19) of Appendix A, corresponding to the specific surface area, permeability and tortuosity, respectively. We have (Marion, 1990),

$$\kappa = \frac{\phi^3}{2s^2\mathcal{T}}, \tag{5}$$

where

$$\phi = \begin{cases} \phi_s - C(1-\phi_c), & C \le \phi_s, \\ C\phi_c, & C > \phi_s, \end{cases} \tag{6}$$

$$s = \begin{cases} s_s + Cs_c, & C \le \phi_s, \\ s_s \dfrac{1-C}{1-\phi_s} + Cs_c, & C > \phi_s, \end{cases} \tag{7}$$

$$\mathcal{T} = \begin{cases} \mathcal{T}_s \left[1 + \dfrac{C}{\phi_s}(\mathcal{T}_c - 1)\right], & C \le \phi_s, \\ \mathcal{T}_c \left[1 + \dfrac{\mathcal{T}_s - 1}{\phi_s - 1}(C-1)\right], & C > \phi_s, \end{cases} \tag{8}$$

where

$$s_s = \frac{3(1-\phi_s)}{r_s}, \quad s_c = \frac{3(1-\phi_c)}{r_c} \tag{9}$$

and

$$\mathcal{T}_s = 1 - 0.5\left(1 - \frac{1}{\phi_s}\right), \quad \mathcal{T}_c = 1 - 0.5\left(1 - \frac{1}{\phi_c}\right). \tag{10}$$

Actually, Marion (1990) gives the equation $\kappa = \phi^3/(k_0\mathcal{T}^2 s^2)$, where $\mathcal{T} = l/L$ is the square root of the tortuosity defined in the present work [see equation (A.10) in Appendix A] and k_0 is an empirical constant. Basically, apart from the clay content C, the free parameters are r_s, r_c, ϕ_s and ϕ_c. If we assume $\phi_s = \phi_c$, we have the same number of free parameters of model 1, i.e., the radii of the sand and clay particles. In this case

$$\phi_s = \begin{cases} \dfrac{\phi + C}{1 + C}, & C \le \phi_s, \\ \phi/C, & C > \phi_s. \end{cases} \tag{11}$$

Note this limitation of equation (10): The porosity and therefore the tortuosity is grain-size independent for an ordered packing of identical spheres, but this is not true for a random arrangement of spheres, which is the case of rocks.

Another approach to obtain permeability (not used here) is based on specific surface area s, if available from laboratory measurements. In this case, one can avoid using the clay content. The permeability is given by equation (A.13). Surface areas, s_m, are usually given in m^2/g (mass normalized) (see Kuila and Prasad, 2013), where g is the gravity constant. The volume normalized surface area is then $s = s_m\rho$, where ρ is the density of the rock.

2.4 Model 4

The Kozeny-Carman equation is based on ideal geometries of the pore space and solid component. This is clear in the demonstration given in Appendix A, when we obtain the specific surface area. The fact that grains are non-spherical and non-uniform in size and the grain packing is non-uniform are not considered. These issues are all directly or indirectly related to mineral composition, and it therefore makes sense that a combination of porosity and mineral abundances would lead to an improved permeability estimation.

Clay particles (smectite, kaolinite, montmorillonite, illite, chlorite, etc.) are much lesser in size than silt particles, even though all soils with particles size less than 60 μm are classified as either silt or clay; specifically the silt grain diameter ranges from 4 μm to 60 μm and clay less than 4 μm. Feldspars have diameters similar to that of silt particles (Stevens, 1991).

Herron model (Herron, 1987) takes into account the mineralogy composition instead of the radii of the particles. The permeability is given by

$$\log_{10}[\kappa(\mathrm{mdarcy})] = A + 3\log_{10}\phi - 2\log_{10}(1-\phi) + \sum_i B'_i M_i, \tag{12}$$

or

$$\kappa = \frac{\phi^3}{(1-\phi)^2} 10^{A+\sum_i B'_i M_i}, \tag{13}$$

where M_i is the weight fraction of each mineral and B'_i is a constant for each mineral, related somehow to the radii of the particles,

$$A = A_0 + 2F_{\max}, \tag{14}$$

where A_0 is a constant and $F_{\max}$ is the maximum feldspar content. The coefficients used by Herron (1987) are:

Quartz: $B'_1 = 0.1$

Feldspar: $B'_2 = 1$

Calcite: $B'_3 = -2.5$

Kaolinite: $B'_4 = -4.5$

Illite: $B'_5 = -5.5$

Smectite: $B'_6 = -7.5$

The quantity $A_0 = 4.9$ for the area considered by Herron (1987) (Venezuela, Faja del Oricono region), but it has to be calibrated for the specific region. It is a function of the maximum feldspar content in a given zone, which reflects the compositional and textural maturity of the sediment. Herron (1987) estimate A_0 and B'_i from comparisons between air permeability measurements on cores and mineralogy abundances derived from geochemical logging in the same wells.

Note that equation (14) is a Kozeny-Carman equation, since basically

$$\kappa \propto \frac{\phi^3}{(1-\phi)^2}.$$

2.5 Modified models including percolation porosity

There is a percolation porosity, ϕ_c, below which the porosity is disconnected and does not contribute to the flow. The experiments indicate that ϕ_c is of the order of 1 to 3 % (Porter et al, 2013). The percolation effect can be incorporated into the Kozeny-Carman relations simply by replacing ϕ with $\phi - \phi_c$. For instance, model (2) is modified as

$$\frac{1}{\kappa} = \frac{(1-\phi+\phi_c)^2}{a(\phi-\phi_c)^3}\left[(1-C)^2 + C^2 b^2\right]. \tag{15}$$

2.6 Results

Figures 2 and 3 show comparisons between model 1 (vertical permeability) and models 2 and 3, respectively. Model 3 assumes $\phi_s = \phi_c$ [equation (11)]. In the first case, the curves are very similar and only at low porosities differ. As porosity increases, permeability increases, as expected. Small amounts of clay content greatly affects the permeability. For instance, going from $C = 0$ to $C = 0.2$ implies a two orders of magnitude change, from 1 darcy to 10 mdarcy for $\phi = 0.4$. On the other hand, the permeability of model 3 differs substantially with that of the other models. Basically, the permeability of Marion model has negligible variations when the clay content is higher than 0.4, providing higher permeability values than the other models.

Next, we consider thirteen Gulf Coast shaley sandstone samples (Marion, 1990) and compare these data with the results of models 1 and 3. The data is permeability as a function of clay content by weight, C_w. The relation to clay (volume) content, C, is (Marion, 1990),

$$C_w = \begin{cases} \dfrac{C(1-\phi_c)\rho_c}{C(1-\phi_c)\rho_c + (1-\phi_s)\rho_s}, & C \le \phi_s, \\ \dfrac{C(1-\phi_c)\rho_c}{C(1-\phi_c)\rho_c + (1-C)\rho_s}, & C > \phi_s, \end{cases} \tag{16}$$

where ρ_s and ρ_c are the densities of the sand and clay grains, respectively. Inverting for C:

$$C = \begin{cases} \dfrac{C_w(1-\phi_s)\rho_s}{(1-C_w)(1-\phi_c)\rho_c}, & C \leq \phi_s, \\ \dfrac{C_w\rho_s}{(1-\phi_c)\rho_c - C_w[(1-\phi_c)\rho_c - \rho_s]}, & C > \phi_s, \end{cases} \tag{17}$$

We consider the values given in Table 3.2 of Marion (1990), i.e, $\rho_s = 2.568$ g/cm^3, $\rho_c = 2.77$ g/cm^3, $\phi_s = 0.32$, $\phi_c = 0.25$, $\mathcal{T}_s = 1.5$ and $\mathcal{T}_c = 10$. Marion (1990) takes the specific surface areas as a free parameter, but here we use equation (9), i.e., the radii. Moreover, the additional free parameter k_0 in eq. (3.14) of Marion (1990) (not reported) is not used here. To be consistent, the porosity and clay content obtained from model 3 are used for model 1. Figure 4 shows the permeability as a function of clay content, where the black and red lines correspond to equations (5) and (2), respectively. As can be seen, both models yield similar results.

A fit of experimental data reported in Chilingar (1969) is shown in Figure 5, for different mineral compositions from very coarse sand to clay. The radii of the sand and clay particles are $r_s = 150$ μm and $r_c = 5$ μm, respectively. The agreement is satisfactory. Finally, to illustrate the effects of percolation porosity, Figure 6 shows the results corresponding to Figure 2 with $\phi_c = 0.02$. As can be appreciated the curves move to the lower permeabilities.

Nelson (1994) used Herron model to obtain permeability versus porosity and clay content. His Fig. 21 is reproduced here in Figure 7, noting that the A values are not reported in Nelson (1994) (here we take $F_{\max} = M_2$) and that the B values used by Nelson in his eq. (8) are not the same of those reported in his Fig. 21, which should be B' [see Herron (1987), his eqs. (4) and (5)]. The equivalence is given by $\log_{10}[\exp(\sum B_i M_i)] = \sum B'_i M_i$ or $B_i = 2.3026 B'_i$. Figure 7 also shows a curve (dotted line) obtained with our equation (2) for case 4, where $C = 0.16$ (kaolinite), using r_s = 50 μm and $r_c = 5$ μm. This curve coincides with that of case 4. To obtain it, we have converted weight fraction to volume fraction using the equations in Appendix C. The densities of the different minerals are: $\rho_s = 2.65$ g/cm^3, $\rho_{fp} = 2.62$ g/cm^3, $\rho_c =$ 2.71 g/cm^3, $\rho_k = 1.58$ g/cm^3, $\rho_{il} = 2.7$ g/cm^3, $\rho_{sm} = 2.4$ g/cm^3, $\rho_{ch} = 2.8$ g/cm^3, for quartz, feldspar, calcite, kaolinite, illite, smectite and chlorite, respectively.

Herron B'_i values are not universal and calibration is required for each area. An example is the following: Let us consider the experiment values of Fig. 5 in Mesri and Olson (1971), which represents the void ratio, e, as a function of the hydraulic permeability, K, for three sodium clays in water, i.e., smectite, illite and kaolinite. Illite is about 200 times more pervious than smectite, and kaolinite is about 200000 times more pervious, at the same void ratio. Porosity and void ratio are related as $\phi = e/(1+e)$, while the absolute permeability is

$$\kappa = \frac{\eta_w K}{g \rho_w},$$

where $\eta_w = 0.001$ Pa s is the viscosity of water, $\rho_w = 1000$ kg/m^3 is water density, and $g = 9.86$ m/s^2 is the gravity constant. We use equation (12) for each clay, in the form

$$\log_{10}[\kappa(\mathrm{mdarcy})] = A + 3\log_{10}\phi - 2\log_{10}(1-\phi) + B', \qquad (18)$$

where B' is Herron coefficient. Figure 8 shows the match between the experimental values and the results of equation (18) with $A = 4.3$, $B' = -7.5$ (smectite), $B' = -5.5$ (illite), and $B' = -3$ (kaolinite), which are quite similar to Herron values.

In the following examples, we adopt Herron B' values. Next, we consider ten wells whose data are given Tables 1 and 2 of Liu et al. (2016), where the illite/smectite mixed layer has been decomposed into illite and smectite. Permeability has been measured with water. Plagioclase is a series of tectosilicate (framework silicate) minerals within the feldspar group, so we included this mineral into the feldspar composition. Table 1 here shows the mineral composition, porosity and permeability at the ten wells. We take $A_0 = 3.5$, $F_{\max}$ = feldspar weight percent (see Table 1) divided by 100 and assume that chlorite has a coefficient $B'_7 = -6$. Figure 9 compares the experimental data to the model results, where it can be seen that the match with Herron model is satisfactory. The blue curve corresponds to equation (2), where we have converted weight fractions to volume fractions and assumed that clay content is given by the sum of the kaolinite, illite, smectite and chlorite fractions. In this case, $r_s = 50$ μm and $r_c = 0.9$ μm.

Klimentos and McCann (1990) provide a complete set of petrographic data for a shaley sandstone (their Table 2, rock sample A6BP), where we consider the X-ray diffraction values. Porosity is 15.4 %, permeability is 52.4 mdarcy, the average (clastic) grain size is 330 μm, and the clay grain size is less than 2 μm. The volume fractions are: quartz: 53 %, feldspar: 32 %, kaolinite: 13.5 % and illite: 1.5 %, so that the clay content is $C =$ 15 % (kaolinite plus illite). On the basis of the mineral densities indicated above, the weight fractions are $M_1 = 56.2$ %, $M_2 = 33.6$ %, $M_4 = 8.5$ % and $M_5 = 1.7$ %. Model 1 provides a perfect fit with $r_s = 330$ μm and $r_c = 3.2$ μm, which are reasonable values provided the highly idealized assumptions. On the other hand, Herron model yields a perfect fit with $A_0 = 3.42$.

Finally, we consider the data of Backeberg et al. (2017). Table 2 shows the composition of samples #2 and #4 given in their Table 1, together with the porosity, permeabilities and Herron coefficients B'. The reported permeability was measured with water; surprisingly they obtained a lower value for argon permeability, in contrast with the Klinkenberg effect (e.g., Tanikawa and Shimamoto, 2006). In order to use Herron equation (12), the volume composition has to be converted to solid volume composition and then to weight composition using equation (C.1). The B' values of quartz, calcite, illite, kaolinite and smectite in Table 2 are taken from Herron (1987). Plagioclase and muscovite are treated as feldspar, and dolomite, pyrite and trace minerals as calcite, since they tend to block the flow. The organic matter [kerogen as reported by Backeberg et al. (2017)] is part of the pore space, which has been obtained with the QEMSCAN measurement (Quantitative Evaluation of Minerals by SCANning electron microscopy), to be consistent with the reported volume compositions. With the values given in Table 2, we can obtain a perfect fit of the experimental permeabilities with equations (2) and (12), by setting for sample #2: $r_s = 50$ μm, $r_c = 0.044$ μm, $A_0 = 2.65$, $F_{\max} = 0.0862$; sample #4: $r_s = 50$ μm, $r_c = 0.014$ μm, $A_0 = 1.68$, $F_{\max} = 0.0891$, where $F_{\max}$ is the feldspar proportion given by the sum of the plagioclase and muscovite proportions. Clay content for equation (2) is the sum of the illite, kaolinite and smectite proportions, after proper normalization. Bulk densities of 2.52 g/cm^3 and 2.53 g/cm^3 are obtained, against the measured values 2.52 g/cm^3 and 2.6 g/cm^3, respectively for samples #2 and #4. Figure 10 shows a fit by assuming a common value $r_c = 0.02$ μm for Model 1 and $A_0 = 2$ for Herron model. Both models yield the same result.

Another technique introduced by Herron et al. (1998, 2002) evaluates permeability based on the lambda parameter, which is a measure of the effective diameter of dynamically connected pores, that can be approximated from the surface-to-pore-volume ratio. The surface-to-pore-volume ratio can be computed from mineralogy data. The other required input data are the total porosity, the matrix density, and Archie's cementation exponent.

Methods based on the Kozeny-Carman equation require defined values of porosity, grain radii, surface area, etc., in order to be applied. Other alternative techniques, such as neural networks, do not require these data. Regarding hydrocarbon exploration, several works using this technique have been published. Helle et al. (2001) and Qadrouh et al (2019), for instance, have predicted porosity and permeability from wireline logs using artificial neural networks. Both techniques can be integrated to provide more reliable results.

3 Conclusions

We have compared four expressions for permeability of the Kozeny-Carman family of equations, which are based on physical parameters such as porosity, grain and pore sizes, tortuosity and mineral composition. This aspect makes this equation predictive unlike simple polynomial fittings. The use of geochemical mineralogy represents a significant improvement in formation characterization over that of geophysical log data alone. The model to be used for a specific case history depends on the data for calibration. Models based on grain radii and/or surface area and clay content are the most common. If, in addition, mineral composition of clays is available, Herron model provides a better estimation of permeability. All models can be applied to sandstones and shales and mixed compositions of sand and clay. Although the geometrical characteristics of the porous rock are idealized, the equations can be used, with proper calibration, to obtain reliable estimates of permeability. The examples presented here show that this estimation is possible.

References

Adams, A., Nordquist, T. J., Germaine, J. T., and Flemings, P. B., 2016, Permeability anisotropy and resistivity anisotropy of mechanically compressed mudrocks, Canadian Geotechnical Journal, 53(9), 1474-1482.

Al Ismail, M. I., and Zoback, M. D., 2016, Effects of rock mineralogy and pore structure on stress-dependent permeability of shale samples, Philos. Trans. A. Math. Phys. Eng. Sci., 374 (2078), 20150428

Backeberg, N. R., Iacoviello, F., Rittner, M., Mitchell, T, M., Jones, A. P., Day, R., Wheeler, J., Shearing, P. R., Vermeesch, P., and Striolo, A., 2017, Quantifying the anisotropy and tortuosity of permeable pathways in clay-rich mudstones using models based on X-ray tomography, Scientific Reports, 7, 14838; DOI:10.1038/s41598-017-14810-1.

Backus, G. E., 1962, Long-wave elastic anisotropy produced by horizontal layering, J. Geophys. Res., 67, 4427-4440.

Bernabé, Y. B., Mok, U., and Evan, B., 2003, Permeability-porosity relationships in rocks subjected to various evolution processes, Pure appl. geophys, 160, 937–960.

Biot, M. A., 1962, Mechanics of deformation and acoustic propagation in porous media: J. Appl. Phys., 33, 1482-1498.

Carcione, J. M., 2014, Wave Fields in Real Media. Theory and numerical simulation of wave propagation in anisotropic, anelastic, porous and electromagnetic media, Elsevier. (Third edition, extended and revised).

Carcione, J. M., Gurevich, B. and Cavallini, F., 2000, A generalized Biot-Gassmann model for the acoustic properties of shaley sandstones. Geophys. Prosp., 48, 539-557.

Carman, P. C., 1961, L' écoulement des gaz á travers les milieux poreux, Bibliothéque des Sciences et Techniques Nucléaires, Presses Universitaires de France, Paris.

Chillingar, G. V., 1963, Relationship between porosity, permeability, and surface areas of sediments, Journal of Sedimentary Research 33 (3), 759-765.

Chilingar. G. V., 1969, Deltaic and Shallow Marine Deposits. L.M.J.U. van Straaten, ed., Elsevier, Amsterdam.

Clennell, M. B., Dewhurst, D. N., Brown, K. M., and Westbrook, G. K., 1999, Permeability anisotropy of consolidated clays, Geol. Soc. Lond. Spec. Publ., 158, 79-96.

Dullien, F. A. L., 1991, One and two phase flow in porous media and pore structure. In Physics of Granular Media, Bideau D., and Dodds, J. eds.. Nova Science Publishers Inc., 173-214.

Fabricius, I. L., Baechle, G., Eberli, G. P., and Weger, 2007, Estimating permeability of carbonate rocks from porosity and v_P/v_S, Geophysics, 72, E185-E191.

Han, T., Best, A. I., Sothcott, J., and MacGregor, L., 2011, Joint elastic-electrical properties of reservoir sandstones and their relationships with petrophysical parameters, Geophys. Prosp., 59, 518-535.

Helle, H. B., Bhatt, A., and Ursin, B., 2001, Porosity and permeability prediction from wireline logs using artificial neural networks, Geophysical Prospecting, 2001, 49, 431-444.

Herron M. M., 1987, Estimating the intrinsic permeability of clastic sediments from geochemical Data, Transactions of the SPWLA 28 the Annual Logging Symposium, London 1987, UK, paper HH.

Herron, M. M., Johnson, D. L., and Schwartz, L. M., 1998, A Robust permeability estimator for siliciclastics, paper SPE 49301 presented at the 1998 SPE Annual Technical Conference and Exhibition, New Orleans 1998, 27-30 September.

Herron, M. M., Herron, S. L., Grau, J. A., Seleznev, N. V., Philips, J., El Sherif, A., Farag, S., Horkowitz, J. P., Neville, T. J., and Kai, H., 2002, Real-time petrophysical analysis in siliciclastics from the integration of spectroscopy and triple-combo logging. In: Proc. SPE Ann. Technical Conference and Exhibition, 29 September-2 October 2002, San Antonio, USA, Society of Petroleum Engineers, DOI: 10.2118/77631-MS.

Klimentos, T., and C. McCann, 1990, Relationships between compressional wave attenuation, porosity, clay content, and permeability of sandstones, Geophysics, 55, 998-1014.

Kozeny, J., 1927, Über kapillare leitung desWassers im Boden: Sitzungsberichte derWienerAkademie desWissenschaften, 136, 271-306.

Kuila, U., and Prasad, M, 2013, Specific surface area and pore-size distribution in clays and shales, Geophys Prosp., 61, 341-362.

Lamb, H., 1945, Hydrodynamics, Dover, New York, pp. 152-156.

Liu, G., Li, S., Gu, D., Lu, Y., and Asamoah, E., 2016, Experimental study of petrophysical properties of a tight formation by considering the clay minerals and flow sensitivities, Earth Sci. Res. J., 20, B1-B6.

Ma, J., Review of permeability evolution model for fractured porous media, 2015, Journal of Rock Mechanics and Geotechnical Engineering, 7, 351-357.

Marion, D., 1990, Acoustical, mechanical and transport properties of sediments and granular materials, Ph.D. thesis, Stanford University.

Mesri, G., and Olson, R. E., 1971, Mechanisms controlling the permeability of clays, Clays and Clay Minerals, 19, 151-158.

Mortensen, J., Engstrøm, F., and Lind, I., 1998, The relation among porosity, permeability, and specific surface of chalk from the Gorm field, Danish North Sea: SPE Reservoir Evaluation &Engineering, 1, 245-251.

Nelson, J. T., 1988. Acoustic emission in a fluid saturated heterogeneous porous layer with application to hydraulic fracture (PhD thesis), Lawrence Berkeley Laboratory, University of California

Nelson, P, 1994, Permeability-porosity relationships in sedimentary rocks, The Log Analyst, 35/3, 38-62.

Neuzil, C. E., 1994, How permeable are clays and shales?, Water Resources Research, 30(2), 145-150.

Porter, L. B., Ritzi, R. W., Mastera, L. J., Dominic, D. F., and Ghanbarian-Alavijeh, B., 2013, The Kozeny-Carman equation with a percolation threshold, Ground Water, 51, 92-99.

Qadrouh, A. N., Carcione, J. M., Alajmi, M., and Alyousif, M. M., 2019, A tutorial on machine learning with geophysical applications, submitted to Bull. Geof. Teor. Appl.

Stevens, R. L., 1991, Grain-size distribution of quartz and feldspar extracts and implications for flocculation processes Geo-Marinc Lettcrs, 11, 162-165.

Savioli, G. B., Santos, J. E., Carcione, J. M., and Gei, D., 2016, A model for CO2 storage and seismic monitoring combining multiphase fluid flow and wave propagation simulators. The Sleipner-field case, Computational Geosciences, DOI 10.1007/s10596-016-9607-y.

Sinha, S., Hardy, R. J., Blois, G., Best, J. L., Sambrook Smith, G. H., 2017, A numerical investigation into the importance of bed permeability on determining flow structures over river dunes, Water Resources Research, 53, 3067-3086.

Tanikawa, W., and Shimamoto, T., 2006, Klinkenberg effect for gas permeability and its comparison to water permeability for porous sedimentary rocks, Hydrol. Earth Syst. Sci. Discuss., 3, 1315-1338,

Tiab, D., and Donaldson, E. C., 2012, Petrophysics.

Appendix A A demonstration of the Kozeny-Carman equation

Let us assume a cylindrical element of Newtonian fluid of length L and radius r flowing in a pipe of radius $r_0 > r$ along the x axis (see Figure 11). The pressure difference between the two faces is dp. The pressure p and viscous force τ compensate (the element is not accelerating). The pressure acts on the surface of the faces and the viscous force acts on the lateral surface given by πr^2 and $2\pi rL$, respectively. Then, the balance is $\pi r^2 p - (p - dp)\pi r^2 - 2\pi rL\tau = 0$, or

$$\frac{dp}{L} = 2\tau r. \tag{A.1}$$

Since dp does not depend on r, it is $\tau \propto r$ (τ vanishes at $r = 0$).
The shear stress obeys a dashpot-like constitutive equation,

$$\tau = -\eta \partial_r v, \tag{A.2}$$

where v is the flow velocity, η is the fluid viscosity, r is the radial coordinate and ∂_r denotes the partial derivative with respect to r. Since the velocity decreases from the pipe centre to zero at the pipe wall, we need to include the minus sign ($\partial_r v < 0$ gives $\tau > 0$). Combining equations (A.1) and (A.2) yields $\partial_r v = -dp/(2\eta L)$, which after integration gives

$$v = -\left(\frac{dp}{4\eta L}\right) r^2 + c, \tag{A.3}$$

where c is a constant. Since $v(r_0) = 0$ (the fluid is welded to the pipe at the wall), we have

$$v = v_{\max}\left(1 - \frac{r^2}{r_0^2}\right), \quad v_{\max} = \frac{dp\; r_0^2}{4\eta L}. \tag{A.4}$$

Integration of the velocity profile on the transverse section of the pipe yields the flow rate,

$$Q = \int_0^{r_0} \pi r v(r) dr = \frac{1}{2}\pi v_{\max} r_0^2 = \frac{\pi r_0^4 dp}{8\eta L}, \tag{A.5}$$

where we used equation (A.4). This is the so-called Hagen-Poiseuille law.

A.1 Permeability

If S is the cross-section area of a porous sample and η is the dynamic viscosity, the permeability κ obeys

$$Q = S\frac{\kappa}{\eta}\frac{dp}{L}, \tag{A.6}$$

while porosity is given by

$$\phi = \frac{\pi r_0^2 L}{SL} = \frac{\pi r_0^2}{S}. \tag{A.7}$$

Using this equation and comparing equations (A.5) and (A.6), we obtain

$$\kappa = \frac{\phi r_0^2}{8}. \tag{A.8}$$

If the pipe makes an angle θ with the x-axis and its length is l, i.e., $\sin\theta = L/l$, the porosity is

$$\phi = \frac{\pi r_0^2 l}{SL} = \frac{\pi r_0^2 \sqrt{\mathcal{T}}}{S}, \tag{A.9}$$

where

$$\mathcal{T} = \left(\frac{l}{L}\right)^2 = \frac{1}{\sin^2\theta} \tag{A.10}$$

is the tortuosity. There is another definition of tortuosity as l/L . The definition here is such that the resistivity formation factor F is almost proportional to $\mathcal{T}$ (Tiab and Donaldson, 2012; eq. 3.21). Now, the pressure gradient becomes $dp/l = dp/(L\sqrt{\mathcal{T}})$ and it is easy to show that the permeability becomes

$$\kappa = \frac{\phi r_0^2}{8\mathcal{T}}. \tag{A.11}$$

This equation can be general if r_0 is an effective pore radius and $\mathcal{T} \geq 1$ can be obtained from experiments.

The specific surface area s is defined as the area of the pore, $2\pi r_0 l$, divided by the volume of the sample, SL. Using equation (A.7), it is

$$s = \frac{2\phi}{r_0}. \tag{A.12}$$

Then

$$\kappa = \frac{\phi^3}{2s^2\mathcal{T}} \tag{A.13}$$

(e.g., Chillingar et al., 1963).

Let us consider a sphere of radius r_g (grain), embedded in a cube of length $2r_g$. The porosity obeys $1 - \phi = (4/3)\pi r_g^3/V$, where $V = 8r_g^3$ is the cube volume. The surface area is $s = 4\pi r_g^2/V$, where the numerator is the pore-space area (area of the sphere). Then,

$$s = \frac{3(1-\phi)}{r_g} \tag{A.14}$$

and (A.13) becomes

$$\kappa = \frac{r_g^2}{18\mathcal{T}} \frac{\phi^3}{(1-\phi)^2}, \tag{A.15}$$

which is the Kozeny-Carman equation (Kozeny, 1927; Carman, 1961).

A.2 Expressions of tortuosity

The Kozeny equation (A.13) can be recast as $\kappa = c\phi^3/s^2$, where c is the Kozeny factor (Fabricius et al., 2007). For straight 3D interpenetrating tubes, the tortuosity is given by

$$\mathcal{T} = 2 + 2\cos\left[\frac{1}{3}\arccos\left(\frac{64\phi}{\pi^3} - 1\right) + \frac{4}{3}\pi\right] \tag{A.16}$$

(Mortensen et al., 1998), where $\mathcal{T}$ decreases from 3 to 2 as ϕ increases from 0.05 to 0.5 A simple expression of tortuosity for grains has been obtained by Berryman (1980) in the framework of Biot's theory of poroelasticity. Nelson (1988) shows that the Biot effective densities are

$$\begin{aligned} \rho_{11} &= (1-\phi)\rho_s + \phi\rho_f(\mathcal{T} - 1), \\ \rho_{12} &= -\phi\rho_f(\mathcal{T} - 1), \\ \rho_{22} &= \phi\rho_f\mathcal{T}, \end{aligned} \tag{A.17}$$

where ρ_f and ρ_s are the fluid and grain densities (see also Carcione (2014) for a complete demonstration). Interpreting ρ_{11} as

$$\rho_{11} = (1-\phi)(\rho_s + \gamma\rho_f), \tag{A.18}$$

where $\gamma\rho_f$ is the induced mass due to the oscillations of the solid particles in the fluid (Lamb, 1945), we obtain

$$\mathcal{T} = 1 - \gamma\left(1 - \frac{1}{\phi}\right). \tag{A.19}$$

For spherical grains ($\gamma = 1/2$), $\mathcal{T}$ decreases from 10 to 1.5 as ϕ increases from 0.05 to 0.5

Appendix B Sand and clay partial permeabilities

To obtain the permeability of the composite medium (sand-clay mixture), we consider an idealized situation when the solid part can be modelled as a dilute concentration of sand and clay spherical particles in the fluid. This situation is realized in the high-porosity limit ($\phi \to 1$). Since the concentration is dilute, each particle can be considered independently from the others. The viscous resistance force for a single sphere of radius r moving in a flow of average velocity v and a fluid viscosity η_f obeys Stokes's law $F = 6\pi\eta_f vr$. Suppose that in a unit volume we have n_ν particles of radius r_ν, $\nu = 1$ (sand grains) or 2 (clay particles). Then, the viscous resistance to the flow by particles of type ν can be written as

$$F_\nu = 6\pi\eta_f v n_\nu r_\nu. \tag{B.1}$$

The density numbers n_ν can be thought of as the total volume of the particles of type ν divided by the volume of a single particle,

$$n_\nu = \frac{\phi_\nu}{\frac{4}{3}\pi r_\nu^3}, \tag{B.2}$$

where

$$\phi_1 = (1-\phi)(1-C), \quad \text{and} \quad \phi_2 = (1-\phi)C \tag{B.3}$$

are the sand and clay proportions, with C the clay content.
Substitution of (B.2) into equation (B.1) yields

$$F_\nu = \frac{9}{2}\eta_f v \phi_\nu r_\nu^{-2},$$

or, for the Biot viscous resistance coefficient,

$$b_\nu = F_\nu \frac{\phi^2}{v} = \frac{9}{2}\eta_f \phi^2 \phi_\nu r_\nu^{-2} \tag{B.4}$$

(Biot, 1962; Carcione, 2014). The quantity

$$\kappa_\nu = \frac{2}{9}\frac{r_\nu^2}{\phi_\nu} \tag{B.5}$$

can be thought of as a partial permeability of the matrix formed by particles of type ν. Hence, $b_\nu = \eta_f \phi^2/\kappa_\nu$, as expected (Biot, 1962).
Equation (B.5) provides an explicit expression for the resistance coefficients in the high-porosity limit. To be consistent with the Kozeny-Carman equations (A.15), we divide the expression for permeability by the factor $10(1-\phi)/\phi^3$ (see Appendix A), which corresponds to a tortuosity of 2.5. Then,

$$\kappa_\nu = \frac{r_\nu^2 \phi^3}{45\phi_\nu(1-\phi)}. \tag{B.6}$$

In the following, ν =1, 2 are identified with sand (s) and clay (c).

Appendix C Conversion from weight fraction to volume fraction and vice versa

Assume n components, each of density ρ_i and weight fraction M_i. Weight fraction is defined as

$$M_i = \frac{\rho_i v_i}{\sum_i \rho_i v_i}, \tag{C.1}$$

where v_i is the volume of each component. Volume fraction is defined as

$$V_i = \frac{v_i}{\sum_i v_i}. \tag{C.2}$$

Then, the ratio between the total volume $v = \sum_i v_i$ to the total mass $m = \sum_i \rho_i v_i$ is

$$\frac{v}{m} = \sum_i \frac{M_i}{\rho_i}. \tag{C.3}$$

It is straightforward to show that

$$V_i = \frac{M_i}{\rho_i} \left(\sum_i \frac{M_i}{\rho_i} \right)^{-1} \tag{C.4}$$

and

$$M_i = \frac{\rho_i V_i}{\sum_i \rho_i V_i} \tag{C.5}$$

Table 1. Mineral composite, porosity and permeability for ten wells of Zhenbei area (China) (Liu et al., 2016).

Well	Quartz	Feldspar	Calcite	Kaolinite	Illite	Smectite	Chlorite	ϕ	κ
Z-1	36	20	25	2.47	7	0.98	8.55	10.23	0.385
Z-2	38	22	18	1.8	10	1.61	8.58	7.84	0.184
Z-3	43	20	17	2.8	8	0.6	8.6	9.13	0.327
Z-4	30	23	22	1.5	14	2.75	6.75	6.637	0.121
Z-5	42	24	12	2.2	10.2	1.9	7.7	7.06	0.149
Z-6	45	21	13	2.31	10	1.8	6.9	8.46	0.251
Z-7	36	23	18	2	11.9	1.28	7.82	8.06	0.214
Z-8	42	19	20	3	7	1.4	7.6	9.85	0.352
Z-9	36	25	15	0.5	14.1	2.7	6.72	6.837	0.132
Z-10	40	20	17	3.2	10.3	1.7	7.8	7.11	0.163

Mineral composition [weight %]; porosity [volume %]; κ [mdarcy].

Table 2. Mineral composition (volume %) and properties (Backeberg et al., 2017).

Sample	#2	#4	ρ (g/cm^3)	B'
Quartz	11.2	9.6	2.65	0.1
Plagioclase	2.9	3.6	2.62	1
Dolomite	2.9	9.6	2.9	- 2.5
Calcite	0.6	1.3	2.71	- 2.5
Muscovite	6.3	5.6	2.81	1
Pyrite	1.3	1.6	4.8	-2.5
Trace minerals	11	4	2.6	-2.5
Porous space	1.5	3.4	1.7	–
Illite	49.8	49	2.7	- 5.5
Kaolinite	8.7	8.6	1.58	- 4.5
Smectite	3.8	3.7	2.4	- 7.5
ϕ (volume %)	1.5	3.4	–	–
κ (ndarcy)	0.35	0.4	–	–

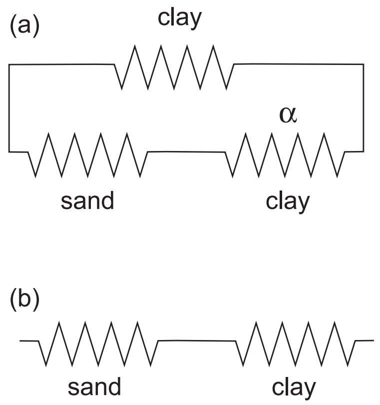

Fig. 1 Electrical-circuit analogy to obtain the horizontal (a) and vertical (b) permeability components. In (a) the sandy part is affected by a clay fraction αC.

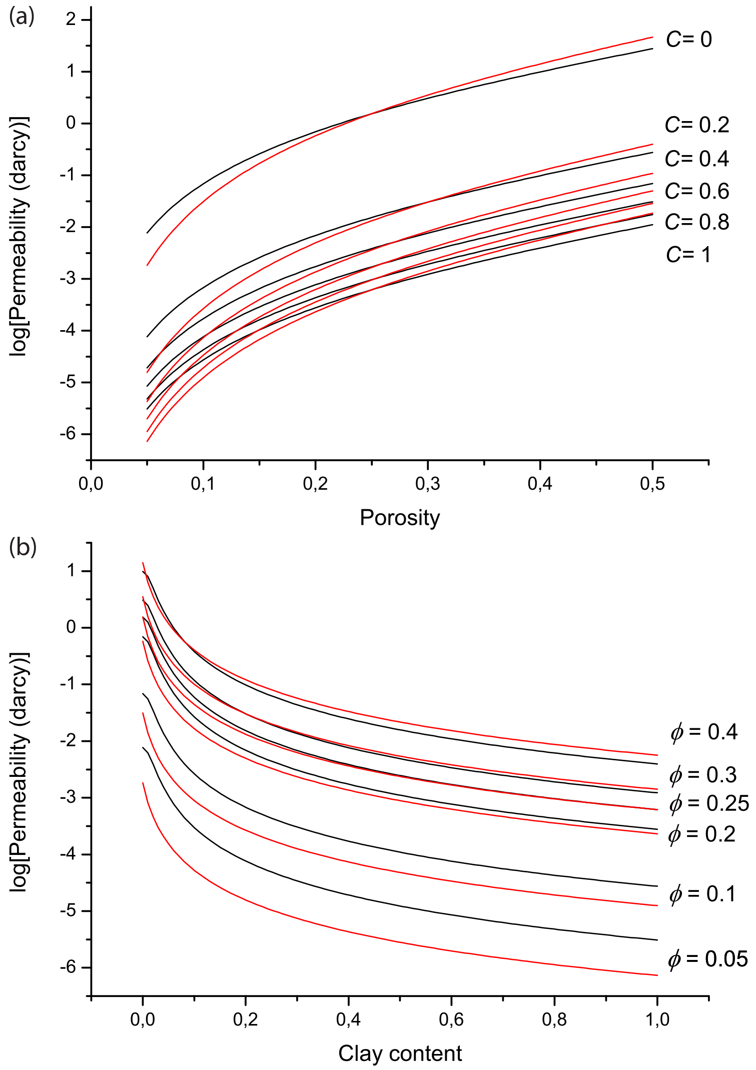

Fig. 2 Permeability versus porosity (a) and clay content (b) for different values of the clay content and porosity, respectively. The black and red lines correspond to equations (2) and (3), respectively (models 1 and 2). The radii of the sand and clay particles are $r_s = 50$ μm and $r_c = 1$ μm, respectively.

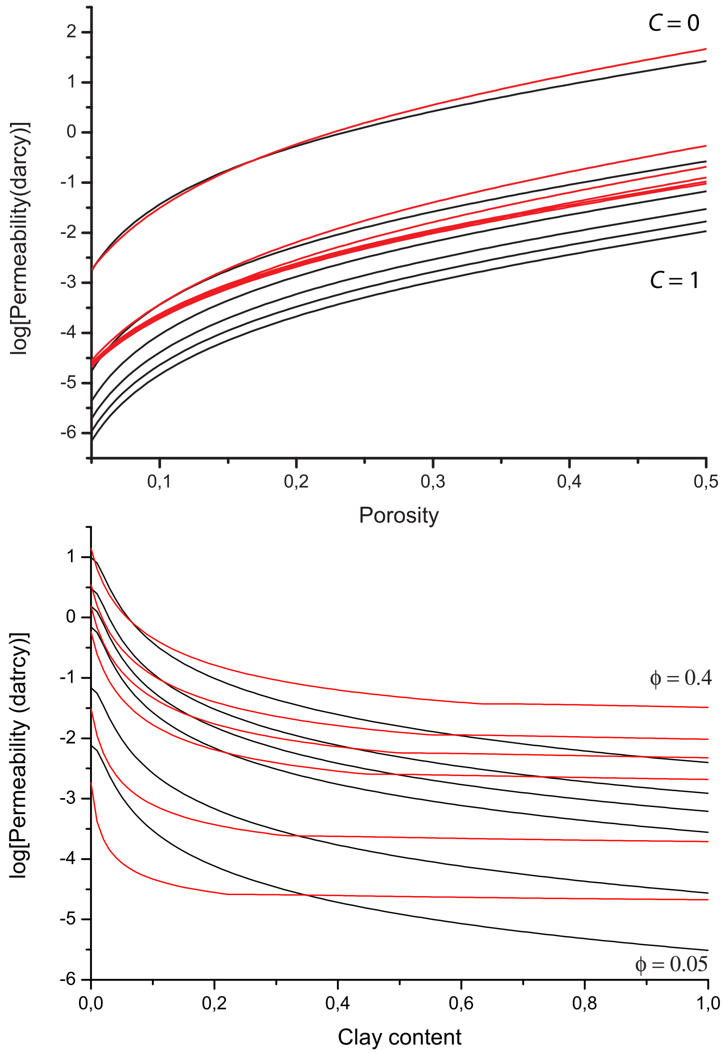

Fig. 3 Permeability versus porosity (a) and clay content (b) for different values of the clay content and porosity, respectively. The black and red lines correspond to equations (2) and (5), respectively (models 1 and 3). The radii of the sand and clay particles are $r_s = 50$ μm and $r_c = 1$ μm, respectively.

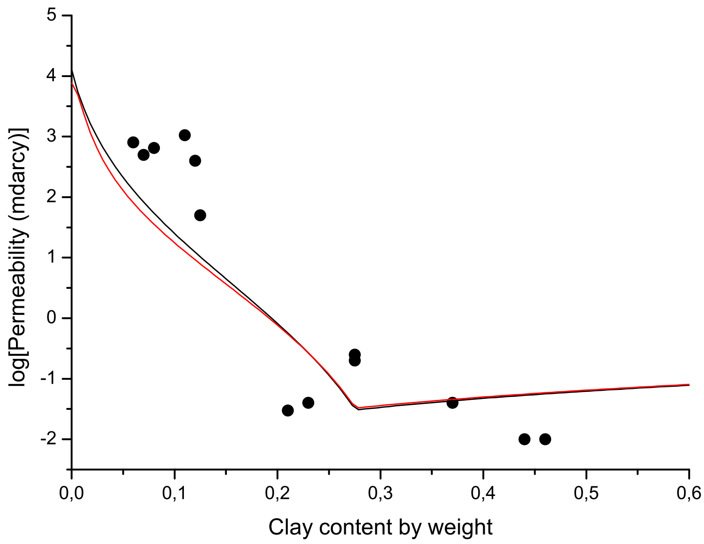

Fig. 4 Permeability versus clay content. The black and red lines correspond to equations (5) (model 3) and (2) (model 1), respectively, and the dots to the experimental data (Marion, 1990). The radii of the sand and clay particles are $r_s = 70$ μm and $r_c = 1$ μm in the first case (model 3), and $r_s = 70$ μm and $r_c = 0.5$ μm in the second case (model 1), respectively.

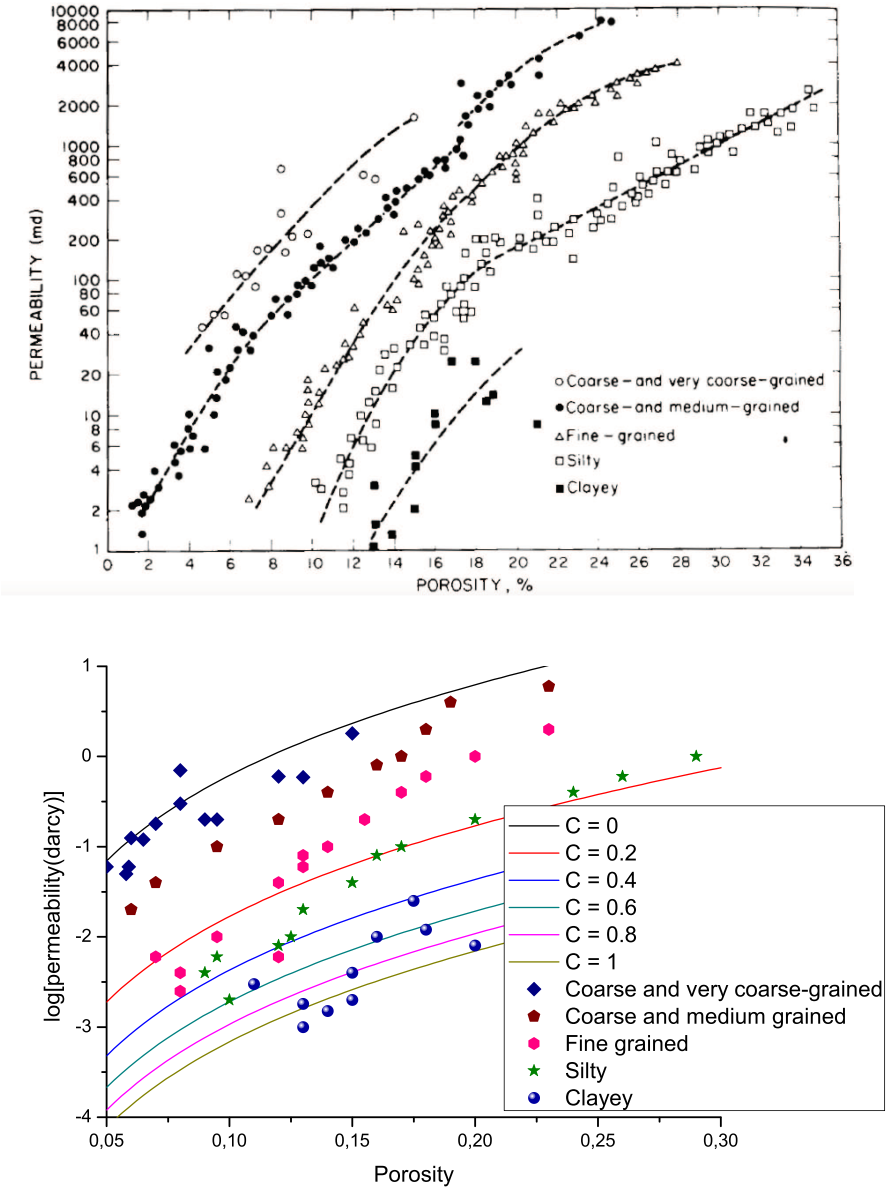

Fig. 5 Comparison with experimental data (Chilingar, 1969) using equation (2) (model 1). The radii of the sand and clay particles are $r_s = 150$ μm and $r_c = 5$ μm, respectively.

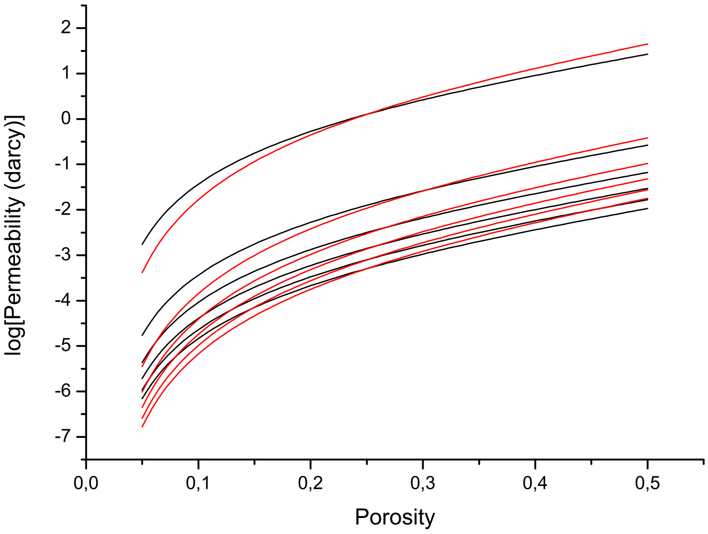

Fig. 6 Permeability versus porosity for different values of the clay content. The black and red lines correspond to equations (2) and (3), respectively (models 1 and 2). The radii of the sand and clay particles are $r_s = 50\ \mu$m and $r_c = 1\ \mu$m, respectively. These curves are affected by a percolation porosity $\phi_c = 0.02$ (compare to Figure 1, where the percolation porosity is zero).

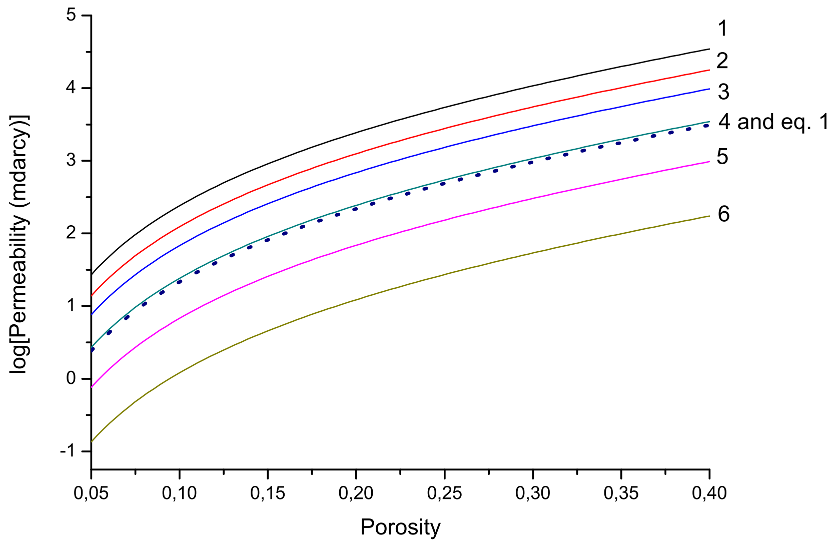

Fig. 7 Permeability versus porosity for different mineralogical compositions, using equation (12) (model 4). The six cases are: Case 1: $M_1 = 0.9$ and $M_2 = 0.1$; Case 2: $M_1 = 1$; Case 3: $M_1 = 0.9$ and $M_3 = 0.1$; Case 4: $M_1 = 0.9$ and $M_4 = 0.1$; Case 5: $M_1 = 0.9$ and $M_5 = 0.1$; Case 6: $M_1 = 0.9$ and $M_6 = 0.1$. The dotted curve obtained from equation (2) (model 1) coincides with that of case 4. The radii of the sand and clay particles in equation (2) are $r_s = 50$ μm and $r_c = 5$ μm, respectively.

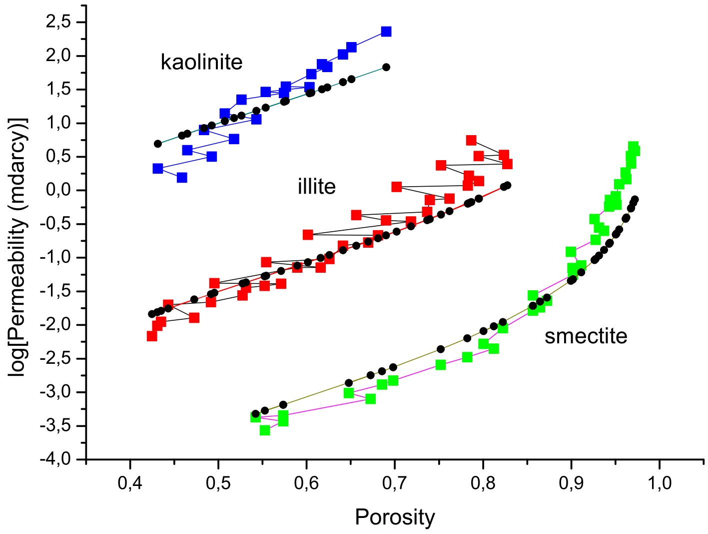

Fig. 8 Comparison between experimental data (square symbols, from Mesri and Olson, 1970) and the results of Herron model (model 4) (solid circles, equation (18)) for three clays.

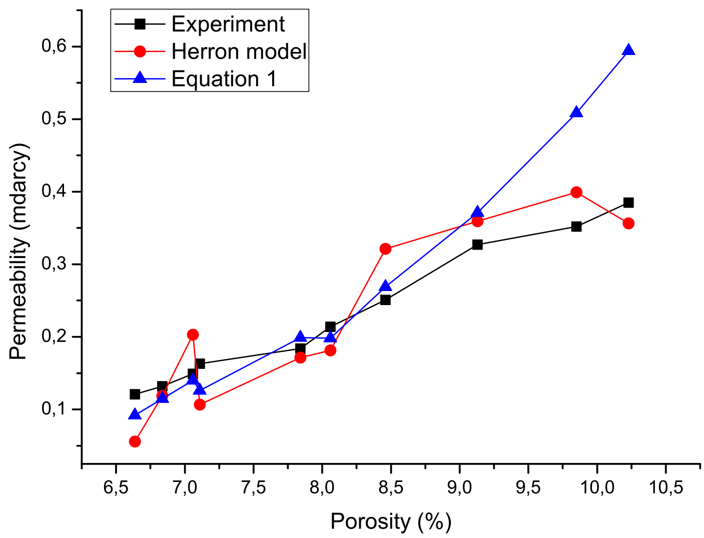

Fig. 9 Comparison between experimental data (black, Liu et al., 2016), the results of Herron model (model 4) (red, equation (12)) based on mineral composition and those of equation (2) (blue).

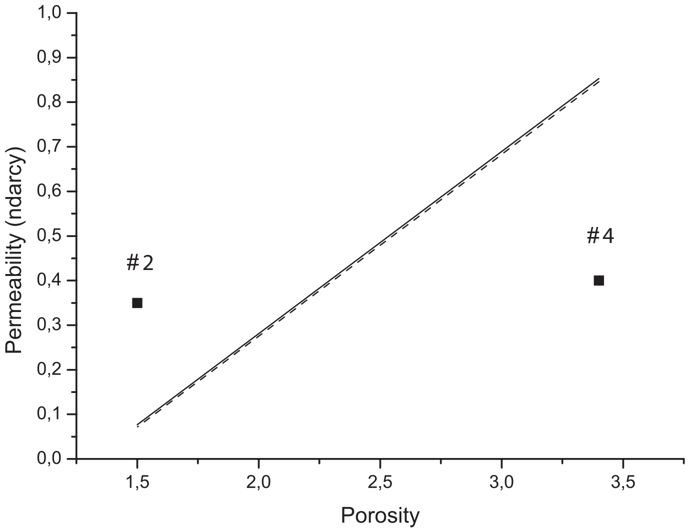

Fig. 10 Comparison between experimental data (symbols) (Backeberg et al., 2017) and the results of equations (2) (model 2, dashed line) and (12) (solid line, Herron, model 4). We assume $r_c = 0.02$ μm for Model 1 and $A_0 = 2$ for Herron model.

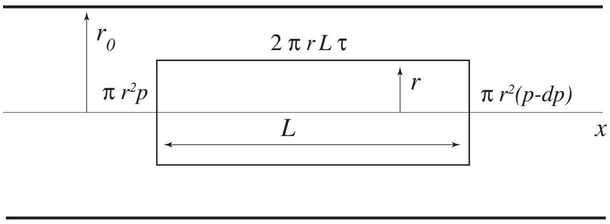

Fig. 11 Initial reference model to obtain permeability as a function of porosity. Balance of forces on a cylindrical element of fluid in a pipe.